

## CHAPTER 162

### PERFORMANCE EVALUATION OF BUOY-MEMBRANE WAVE BARRIERS

M.H. Kim<sup>1</sup>, B.L. Edge<sup>2</sup>, S.T. Kee<sup>3</sup>, and L. Zhang<sup>4</sup>  
Department of Civil Engineering  
Texas A&M University  
College Station, TX 77843, USA

#### ABSTRACT

The interaction of water waves with a tensioned, inextensible, vertical flexible membrane hinged at the sea floor and attached to a solid cylindrical buoy at its top, was investigated in the context of two-dimensional linear wave-body interaction theory. A two-domain boundary element program was developed based on a discrete-membrane dynamic model and simple-source distribution over the entire fluid boundaries. To verify the numerical results, a series of experiments were conducted with two different models in the two-dimensional wave tank. For each model, both surface-piercing and submerged cases were tested. The numerical prediction was generally in good agreement with experimental results except resonance regions. The comparison was improved after including viscous or material damping effects. It is shown that the buoy/membrane system can be a very effective wave barrier if it is properly designed.

#### INTRODUCTION

A flexible membrane can be used as a portable and sacrificial breakwater, containment boom, underwater screen (Huygens et al., 1994), and silt curtain (Sawaragi et al., 1989). It has the advantage of being lightweight, inexpensive, reusable, and rapidly deployable. Since it can be easily removed, we expect minimum environmental impacts on various coastal processes. Using inflatable buoy, it can be air-dropped and self-erected. Its shape and mass can be easily controlled by filling with air or water optimized for various sea conditions (e.g. Ohyama et al., 1989; Broderick & Jenkins, 1993; Zhao, 1994). In this paper, we will particularly focus on the use of floating or submerged buoy/membrane as a breakwater (Thompson et al., 1992).

Most floating breakwaters proposed so far (e.g. Seymour & Hanes, 1979; Sollitt et al., 1986; Isaacson et al., 1994) have been relatively transparent to the incident wave field especially in the long wave regime. In order to improve the performance in long waves, it is necessary for the structure to occupy a major fraction of the water column. In view of this, numerous flap-type or elastic-beam breakwaters have been investigated but they were not greatly successful primarily due to the motion-induced waves in the lee side. The effectiveness of this kind of vertical breakwaters was improved by tuning structural responses (Sollitt et al, 1986; Evans & Linton, 1991; Abul Azm, 1994) or by adjusting structural flexibility (Lee & Chen, 1990; Williams et al., 1991,1992) and porosity (Wang & Ren, 1993).

---

<sup>1</sup> Associate Prof., Dept. of Civil Engrg, Texas A&M Univ., College Station, Texas, 77843

<sup>2</sup> Prof., Dept. of Civil Engrg., Texas A&M Univ., College Station, Texas, 77843

<sup>3</sup> Res. Asst. Dept. of Civil Engrg., Texas A&M Univ., College Station, Texas, 77843.

<sup>4</sup> Res. Asst., Dept. of Civil Engrg., Texas A&M Univ., College Station, Texas, 77843.

In Kim & Kee (1996), the wave interaction with a tensioned vertical flexible membrane hinged or elastically supported at the seabed and the mean free surface was considered. Both analytic and numerical solutions were developed and used to assess the performance with varying various parameters such as membrane tension, length, mass, and mooring stiffness. It was found that almost complete reflection was possible despite large vertically-sinusoidal membrane motions which tended to generate only exponentially decaying local (evanescent) waves in the lee side. Consequently, the efficiency was in general higher than conventional floating breakwaters. The overall performance, however, depended on the magnitude of membrane tension and types of boundary conditions.

In Kee & Kim (1997), more practical buoy-membrane systems were considered. A special two-domain boundary element method was developed to solve the interaction of a rigid buoy and flexible membrane with regular waves. It was observed that diffracted and radiated waves by a buoy tended to diminish the efficiency of the membrane-alone case. However, it was shown that the practical system with a floating buoy can still be highly efficient if it is properly designed.

To validate the numerical results of Kee & Kim (1997), a series of experiments were conducted in a 35-m long, glass-walled two-dimensional wave tank at Texas A&M University. Two different models were tested both in regular and irregular waves. Reasonable agreement was observed between theory and experiment. The representative results of this experimental study are reported in this paper.

**Key Words:** flexible membrane, floating breakwater, submerged breakwater, potential theory, hydroelasticity, two-domain BEM, performance evaluation, model experiment

## THEORY AND NUMERICAL METHOD

The interaction of a buoy/membrane wave barrier with long-crested monochromatic waves is solved in the context of potential theory. Buoy and membrane motions are assumed to be uniform in the longitudinal direction thus allowing two-dimensional analysis. It is also assumed that wave and membrane motions are small so that linear theory may be applicable. For analysis, the Cartesian coordinate system with the origin on the mean free surface and the  $y$  axis positive upward is used. Assuming ideal fluid and harmonic motion of frequency  $\omega$ , the velocity potential can be written as  $\Phi(x, y, t) = \text{Re}[\phi(x, y)e^{-i\omega t}]$ . The velocity potential of a monochromatic incident wave of amplitude  $A$  and wavenumber  $k$ , propagating in the positive  $x$  direction is given by

$$\phi_0 = \frac{-igA \cosh k(y+h)}{\omega \cosh kh} e^{ikx} \quad (1)$$

where  $\omega^2 = kg \tanh kh$  with  $g$  and  $h$  being the gravitational acceleration and water depth, respectively. The complex disturbance velocity potentials,  $\phi_1$  and  $\phi_2$ , in two fluid domains I and II (see Figure 1) satisfy Laplace equation  $\nabla^2 \phi_l = 0, (l = 1, 2)$  and the following linearized free-surface ( $\Gamma_f$ ), bottom ( $\Gamma_b$ ), and radiation conditions:

$$-\omega^2 \phi_l + g \frac{\partial \phi_l}{\partial y} = 0 \quad (\text{on } \Gamma_f) \quad (2)$$

$$\frac{\partial \phi}{\partial n} = 0 \quad (\text{on } \Gamma_b) \tag{3}$$

$$\lim_{|x| \rightarrow \infty} \left( \frac{\partial}{\partial x} \pm ik \right) \begin{pmatrix} \phi_1 \\ \phi_2 \end{pmatrix} = 0 \quad (\text{on } \Gamma_c) \tag{4}$$

where  $\mathbf{n} = (n_x, n_y)$  is the unit outward normal vector.

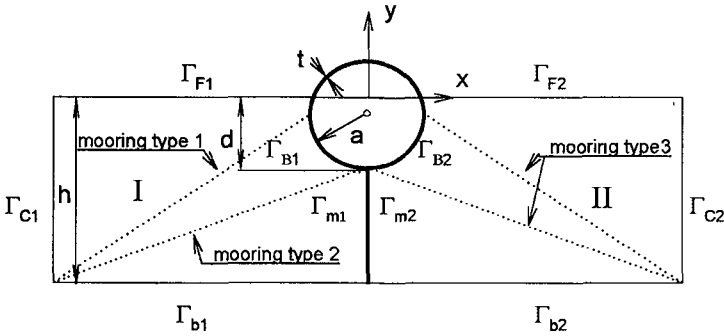


Figure 1. Computational domain.

Under large initial tension, we assume, for simplicity, that the membrane is inextensible and the heave motion of the buoy is negligible. Then the boundary condition on the buoy is

$$\frac{\partial \phi}{\partial n} + i\omega \{ \eta_h n_x + \eta_b n_\theta \} + \delta_{11} \frac{\partial \phi_0}{\partial n} = 0 \quad (\text{on } \Gamma_b) \tag{5}$$

where  $\delta$  is the Kronecker delta function, and  $n_\theta = xn_y - yn_x$ . The symbols  $\eta_h$  and  $\eta_b$  represent complex sway and roll responses respectively. In addition, the disturbance potentials must satisfy the following linearized kinematic and dynamic boundary conditions on the membrane surface:

$$\frac{\partial(\phi_1 + \phi_0)}{\partial x} = \frac{\partial \phi_2}{\partial x} = -i\omega \xi \tag{6}$$

$$\frac{d^2 \xi}{dy^2} + \lambda^2 \xi = \frac{\rho i \omega}{T} (\phi_2 - \phi_1 - \phi_0) \quad (\text{on } \Gamma_m) \tag{7}$$

in which  $\lambda = \omega \sqrt{m/T}$  with  $T$  and  $m$  being the membrane tension and mass per unit length, respectively. In (6) and (7),  $\rho$  is the fluid density, and the harmonic membrane motion  $\Xi(y,t) = \text{Re}[\xi(y)e^{-i\omega t}]$ . The dynamics of the tensioned membrane is modeled as that of the tensioned string which satisfies one-dimensional wave equation. Unlike rigid body hydrodynamics, the body boundary condition on the flexible membrane is not known in advance. Therefore, the

membrane motions and velocity potentials need to be solved simultaneously. If buoy is submerged, the continuity of pressure and normal velocity must be satisfied along the fictitious vertical centerline above buoy:

$$\phi_1 = \phi_2, \quad \frac{\partial \phi_1}{\partial n} = -\frac{\partial \phi_2}{\partial n} \quad \text{at } \Gamma_f \quad (8)$$

To solve the above boundary value problem, a two-domain boundary element method using simple sources along the entire boundary is developed. The details are given in Kee & Kim (1997). Two auxiliary vertical boundaries ( $\Gamma_{e1}$ ) and ( $\Gamma_{e2}$ ) are located sufficiently far from the membrane such that the radiation condition (4) is valid. The discrete membrane equation is given in the following form:

$$\rho i \omega (\phi_{0j} + \phi_{1j} - \phi_{2j}) l_j - T_j \left( \frac{\partial \xi}{\partial \zeta} \right)_j + T_{j+1} \left( \frac{\partial \xi}{\partial \zeta} \right)_{j+1} = -m l_j \omega^2 \xi_j \quad (9)$$

where

$$\left( \frac{\partial \xi}{\partial \zeta} \right)_j = (\xi_j - \xi_{j-1}) / \Delta \zeta_j$$

The symbol  $l_j$  is the length of the  $j$ -th segment, and  $\Delta \zeta_j = \frac{l_j + l_{j+1}}{2}$ . The geometric boundary conditions at the seabed and the top connection point  $(0, -R)$  are

$$\xi = 0 \quad \text{at } z = -h, \quad \xi = \eta_h + R\eta_b \quad \text{at } z = -R \quad (10)$$

The equation (9) can in principle be solved for variable tensions. In the present study, however, we assume that the initial tension  $T$  is much greater than membrane weight or dynamic tension thus can be regarded as constant. The sway-roll coupled equation of buoy motion is given by

$$M(-\omega^2)X = F_p - (K_{HS} + K_m)X - F_T + F_D \quad (11)$$

where  $X = [\eta_h \ \eta_b]^T$ ,  $M$ =buoy mass matrix,  $K_{HS}$ =hydrostatic restoring coefficients,  $K_m$ =mooring stiffness,  $F_p$ =potential force,  $F_D$ =linearized drag force, and  $F_T$ =force at the connection point. The force  $F_T$  caused by membrane tension can be either restoring force or excitation. The detailed expression of these variables is given in Kee & Kim (1997).

## EXPERIMENT

In order to validate the theory and numerical procedure developed in the preceding section, we conducted a series of experiments using a two dimensional wave tank (37-m long, 0.91-m wide, and 1.22m deep) equipped with a dry-back, hinged flap wave maker capable of producing regular and irregular waves (see Figure 2). The wave elevation was measured with a resistance wave gauge having an accuracy of  $\pm 0.1$  cm. A probe measuring incident and reflected wave heights and another probe measuring the transmitted wave heights are placed at 9.14m and 24.38m from the wavemaker, respectively. The wave barrier model was placed at 18.29m from the wavemaker between the two probes. Regular waves were generated by a user-defined time-voltage input to the wave maker. The wave period range used in our experiments was from 0.7 to 2.5. The wave heights used in the experiments range from 3cm to 6cm.

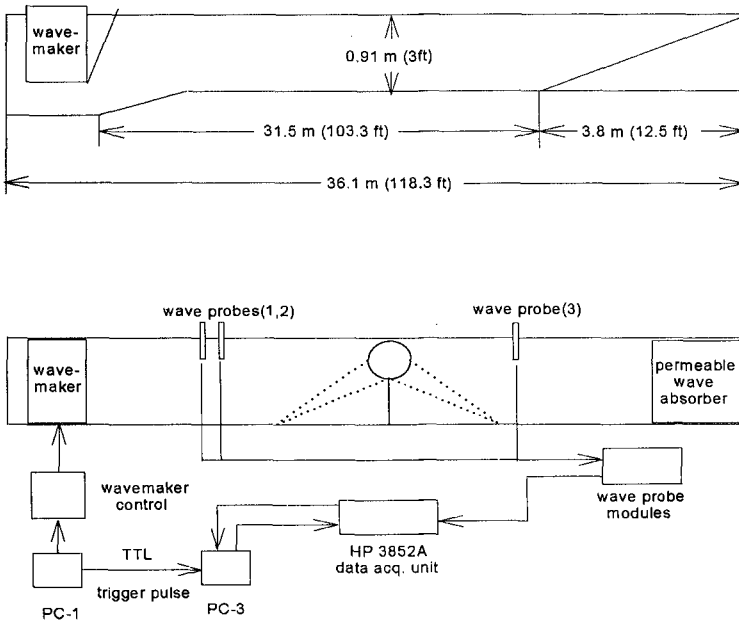


Figure 2. Wave tank and experimental set-up.

A sinusoidal regular wave was generated with the beginning and end of the series attenuated in amplitude. Two models were constructed for the present study. The buoy of model I is relatively small and heavy and made of PVC pipe. The buoy of model II is relatively large and light and made of foam wrapped by plastic sheet. The models consisted of a flexible membrane suspended from a cylindrical buoy and hinged at the sea floor. The flexible membrane was made of a thin stretching-resistant plastic material resembling a plastic tarpaulin. The total length of the buoy with side caps was 86cm. The membrane was attached to the bottom by clamping it between two angle irons which were fastened to the bottom. Four (type 1) or eight (type 3) taut mooring (two at each end) lines are used and they consist of unstretchable steelon-nylon wire that can resist up to 534N and a spring near the bottom connection. When mooring type 3 is used, two taut cables having the same anchoring point are connected to the side and bottom of a buoy, respectively. The stiffness of each spring was measured by applying static loads. The stiffness per length was found to be piece-wise linear as displacement increases. To avoid being slack, each mooring line is slightly pre-tensioned. Table 1 and 2 summarize the principal characteristics of the model I and II used in the experiment. The signal of the incident wave train was obtained (see Figure 3a,b) as it passed the probe toward the membrane breakwater. Then, the reflected wave train was recorded as the reflected waves pass the probe again in the opposite direction. After averaging the wave heights for the incident and reflected, and transmitted wave trains, the reflection coefficient  $R_f$  and transmission coefficient  $T_f$  can be calculated from the ratio of the averaged reflected and transmitted wave height to the averaged incident wave height.



Reflected and transmitted waves were repeatedly reflected from the wave maker and beach as time goes on. In order to minimize the effects of multiple reflection, the fixed single probe method was adopted in favor of moving single probe method and three-probe method (Isaacson, 1991). It is shown in Hagen (1994) that the present method is more reliable than the moving or three-probe methods when nonlinear phenomena or multiple reflections exist. In most of our surface-piercing-buoy experiments, the errors estimated from the energy relation were kept within 10%. The difference can be attributed to viscous, gap, and nonlinear effects, and mooring/material damping etc.

## RESULTS AND DISCUSSION

The boundary element program developed as described in the preceding section was used to predict the performance of surface-piercing or submerged buoy-membrane wave barriers. The computational domain is defined as in Figure 1. The error was calculated from the energy conservation relation  $R_f^2 + T_f^2 = 1$ . It is seen that the errors uniformly decrease as the number of segments is increased.

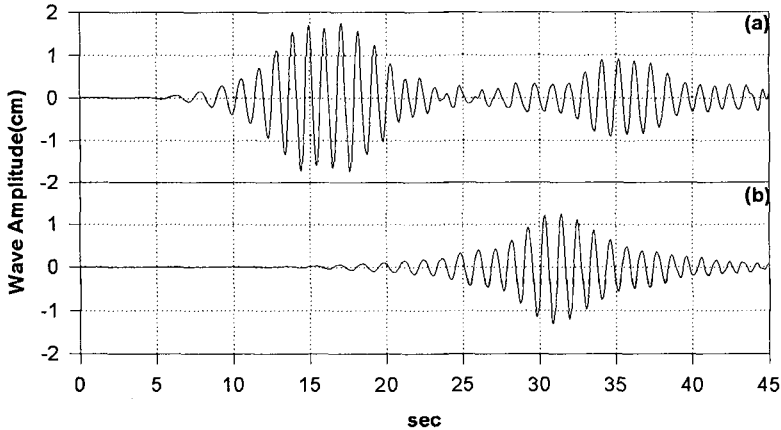


Figure 3. (a) Incident and reflected, and (b) transmitted wave packet for wave period 1.08 sec.

Figure 4 shows comparison between the numerical results and measurements for a surface-piercing buoy/membrane breakwater (model I) without mooring lines. In this experiment, both small and large amplitude waves were used to see the sensitivity to wave heights. As can be seen in the figure, experimental data agree well with the present numerical results. As expected, smaller-amplitude waves correlate better with the linear wave-body-interaction theory. The discrepancy for large-amplitude waves can mainly be attributed to nonlinear effects since it is more pronounced in the high-frequency region. The experimental results satisfied the energy conservation with less than 8% error in the whole frequency range. To account for viscous and material damping effects, 2.5% of the sway and roll critical damping of the cylinder as well as 0%, 2.5%, and 5% of membrane critical damping was included in the cylinder and membrane equations of motions. The results are also plotted in Figure 4. As can be seen in this figure, its effect is not significant in the wave frequency range considered, which is not surprising because the relevant Keulegan-Carpenter (KC) number is smaller than 1.

Figure 5 shows the result of the same case (model I, surface piercing) except that the buoy is moored by a pair of weakly pre-tensioned springs (type 1) located at both ends of the cylinder. As mentioned earlier, the spring exhibited piece-wise nonlinear behavior, and thus the averaged stiffness was used in this computation. The computed results correlate well with the measured data except for the resonance region characterized by the sharp increase of the reflection coefficient. The discrepancy near resonance can mainly be attributed to the increased viscous and nonlinear effects. Actually in this case, we observed large buoy and membrane motions in the experiment. To assess the effects of increased damping due to viscosity and mooring lines, the same damping parameters as in Figure 4 were used in the motion calculation and the results are also shown in Figure 5. It is seen that viscous effects are increased near the resonance region.

In Figure 6, the experimental results for a moored (type 1), submerged wave barrier (model I) are compared with numerical prediction. The overall correlation of the potential theory with experiment is somewhat worse than the surface-piercing cases, indicating that viscous or material damping effects play a more important role for submerged breakwaters. The experimental results do not accurately satisfy the energy relation because of the increased viscous and nonlinear effects. In addition, we observed, especially for short waves (or large  $kh$ ), mild wave breaking above the buoy surface, which can also contribute to energy loss. To see the viscous effects more clearly, we first included the sway drag force on the cylinder through Morison's formula as explained in the preceding section with 5% roll damping ratio. We can see in the figure that its effect is small. To have further insight, we also presented the cases in which the sway and roll damping ratios of the cylinder are 5%, and membrane damping ratio is increased from 0% to 5%. It tends to lower both reflection and transmission coefficients except near  $kh \approx 2.8$ , where reflection increases. The new results with viscosity tend to correlate better with measured data.

Since the buoy of model I is relatively small and heavy, its wave-blocking performance is not very impressive. For comparison, the performance of a similar system with larger and lighter buoy (model II) was also tested and compared with numerical prediction. Figure 7 shows the performance of the model II without mooring for various  $kh$  values. Figure 8 shows the performance of the same system with type 3 mooring lines. In both cases, the predicted results agree well with measured data except the resonance region, where nonlinear effects can be significant. It is also seen that the efficiency in long waves can be significantly enhanced by adding mooring lines. The efficiency for  $kh > 3$  is very high regardless of the presence of mooring lines.

Figure 9 shows the performance of the submerged system (model II) with type-3 mooring in regular waves. Compared to the surface-piercing case, the efficiency in long waves is greatly enhanced, while that in short waves becomes poor. The predicted results again correlate reasonably with measured data. The results of Figure 8 and 9 indicate that high performance can be achieved for a variety of wave conditions if the submerged and surface-piercing systems are combined. Finally, In Figure 10a, the performance of the surface-piercing model II in irregular waves is shown. As a typical operational condition in a partly protected sea, a two-parameter Pierson-Moskowitz spectrum with significant wave height=1.5m and peak period=6.5s was selected. We can see that the transmitted wave spectrum is greatly less than the incident wave spectrum. In this experiment, due to the accumulated multiple reflection from both wave maker and beach, the duration of the time series cannot be long. Therefore, five different time series of 180-s duration were generated and the averaged spectra were presented in Figure 10a. Figures 11a,b show the typical time series of wave elevation recorded by wave probes 1 and 3. Figure 10b shows the performance of the submerged system in irregular waves. For this plot, four different time series are averaged. One of such time series is shown in Figure 11c,d.

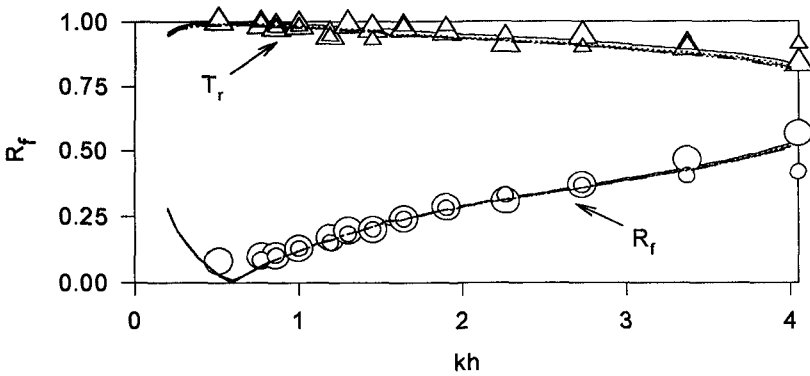


Figure 4. Comparison of the present numerical results with measured data for a surface-piercing membrane breakwater (model I) without mooring lines. Num.  $R_f$  and  $T_r$  (—), Exp. with small wave amplitudes{  $R_f$  (O),  $T_r$  ( $\Delta$ ) }, Exp. with large wave amplitudes{  $R_f$  (o),  $T_r$  ( $\Delta$ )}. Additional lines are for 2.5 % sway and roll damping ratio of the cylinder and membrane damping ratio of 0% (.....), 2.5% (- - - - -), and 5.0% (- · - · - ·).

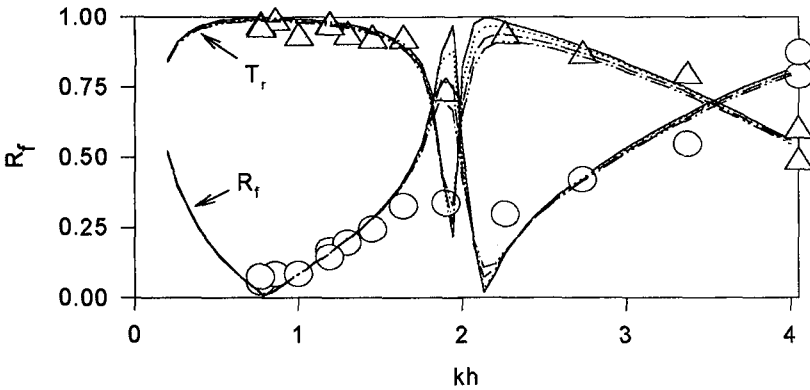


Figure 5. Comparison of the present numerical results with measured data for a surface-piercing membrane breakwater (model I) with type 1 mooring. Num.  $R_f$  and  $T_r$  (—), Exp. {  $R_f$  (O),  $T_r$  ( $\Delta$ ) }. Additional lines are for 2.5 % sway and roll damping ratio of the cylinder and membrane damping ratio 0% (.....), 2.5% (- - - - -), and 5.0% (- · - · - ·).

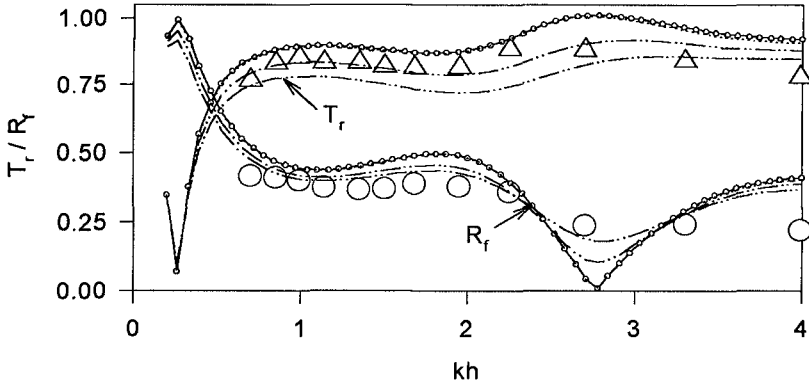


Figure 6. Comparison of the present numerical results with measured data for a fully submerged membrane breakwater (model I) with type 1 mooring. Num.  $R_f$  and  $T_r$  (—), Exp. {  $R_f$  (O) ,  $T_r$  ( $\Delta$ ) }. Circles ( $\circ$ ) represent the results for which Morison equation for sway and 5 % roll damping ratio of the cylinder are used. Additional lines are for 5 % sway and roll damping ratio of the cylinder and membrane damping ratio of, 0 % (.....), 2.5 % (- - - - -), 5.0 %(- · - · - · -)

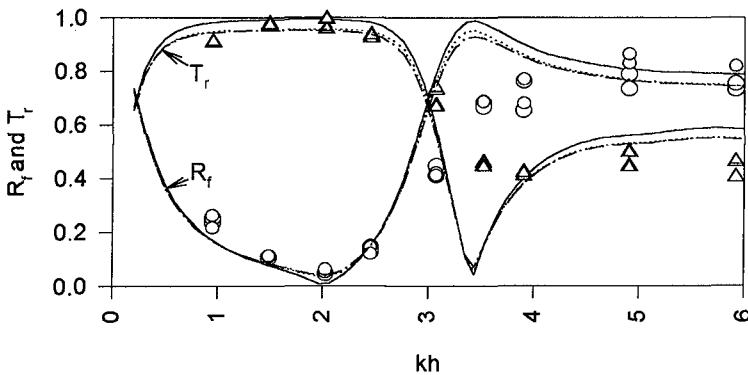


Figure 7. Comparison of the present numerical results with measured data for a surface-piercing membrane breakwater (model II) without mooring lines. Num.  $R_f$  and  $T_r$  (—), Exp. {  $R_f$  (O),  $T_r$  ( $\Delta$ ) }. Additional lines are for 5.0 % sway and roll damping ratio of the cylinder and membrane damping ratio of 5.0% (.....), and 10.% (- - - - -)

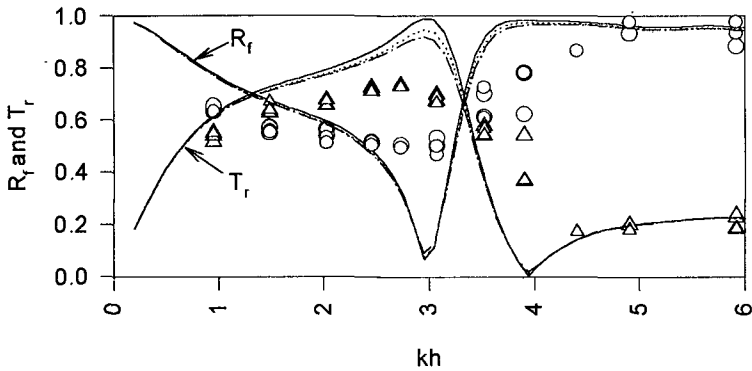


Figure 8. Comparison of the present numerical results with measured data for a surface-piercing membrane breakwater(model II) with type 3 mooring. Num.  $R_r$  and  $T_r$  (—), Exp.  $\{R_r(O), T_r(\Delta)\}$ . Additional lines are for 5.0 % sway and roll damping ratio of the cylinder and membrane damping ratio 5.0 % (.....), 10. % (- - - - -).

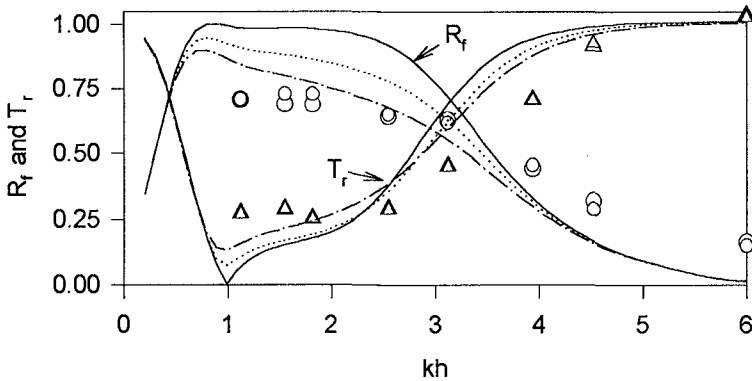


Figure 9. Comparison of the present numerical results with measured data for a fully submerged membrane breakwater (model II) with type 3 mooring. Exp.  $\{R_r(O), T_r(\Delta)\}$ , Num.  $R_r$  and  $T_r$  for sway and roll damping ratio of the cylinder and membrane damping ratio of 0 % (—), 5.0 % (.....), 10.0 % (- - - - -).

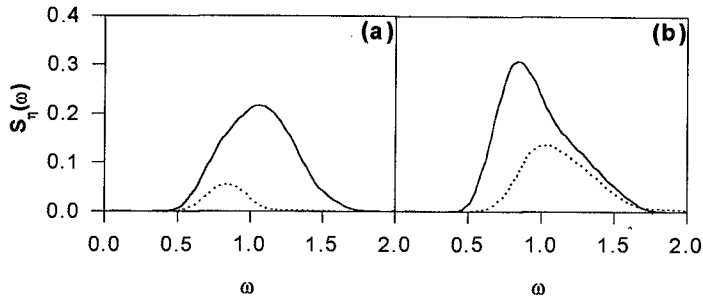


FIG. 10. The spectra of incident (————) and transmitted (·····) irregular waves for a surface-piercing model II (a) and a fully submerged model II (b).

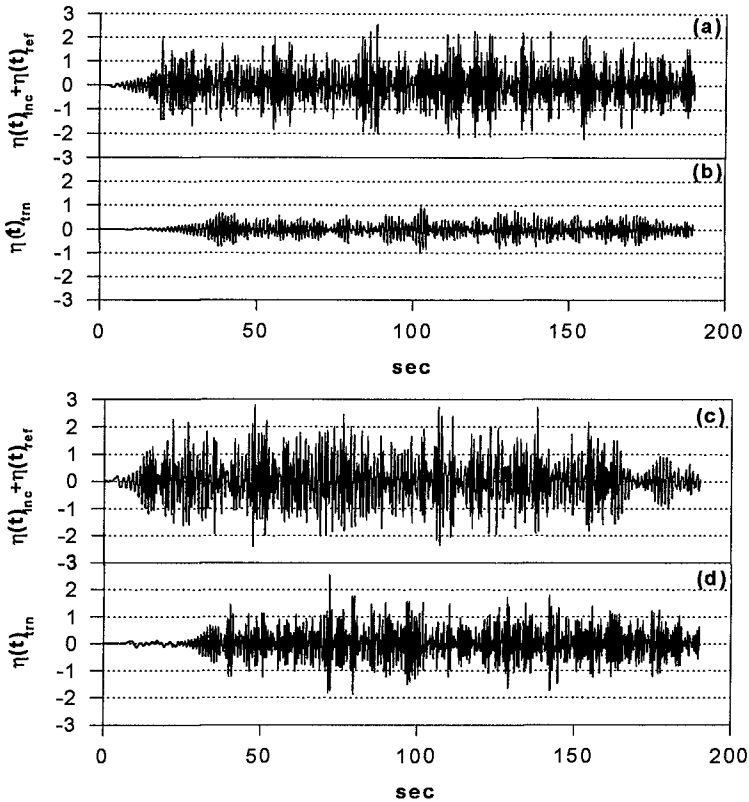


FIG. 11. Time series of incident (a) and transmitted (b) waves for a surface-piercing model II, and incident (c) and transmitted (d) waves for a fully submerged model II

## CONCLUDING REMARKS

The interaction of waves with a tensioned, inextensible, vertical flexible membrane hinged at the sea floor and attached to a rigid cylindrical buoy at its top, was solved in the context of two-dimensional linear wave-body interaction theory. Both submerged and surface-piercing buoy/membrane system were considered. A boundary element program was developed based on a discrete-membrane dynamic model and simple-source distribution over the entire fluid boundaries. A two-domain BEM was employed since the membrane is infinitely thin. Membrane motions and velocity potentials were solved simultaneously because the body-boundary condition on the membrane is not known in advance. The accuracy and convergence of the developed program were verified through comparison with analytic solutions.

To verify the numerical results, a series of experiments were conducted with two different models, in the two-dimensional wave tank. For each model, both surface-piercing and submerged cases were tested. The model I with a small buoy was efficient only for limited wave frequency bands, while the model II with larger and lighter buoy performed well for a wider range of wave conditions. The model II successfully reduced the sea state 3-4 to sea state 2. It was also found that submerged systems can be effective in blocking long waves, while surface-piercing systems are more effective for larger  $kh$  values. The numerical prediction was generally in good agreement with experimental results except resonance regions. The comparison was improved after including viscous or material damping effects.

## ACKNOWLEDGMENT

This research was sponsored by the Korea Research Institute of Ships & Ocean Engineering (KRISO) through a KRISO/TAMU cooperative research program. This work was also partly supported by the Offshore Technology Research Center through the National Science Foundation Engineering Research Centers Program, Grant Number CDR-8721512.

## REFERENCES

- Abul-Azm, A.G. (1994), "Wave diffraction by double flexible breakwaters" *Journal of Applied Ocean Research*, Vol.16, 87-99.
- Broderick, L.L. & Jenkins, C.H. (1993) "Experimental investigation of fluid-filled membrane breakwaters" *ASCE J. of Waterway, Port, Coastal & Ocean Engineering*, Vol 119, #6, 639-656.
- Evans, D.V. & Linton, C.M. (1991) "Submerged Floating Breakwaters" *J. of Offshore Mechanics & Arctic Engr.*, Vol 113, 205-210.
- Hagan, C.L. & Kim, M.H. (1994), "A theoretical/experimental study of a perforated wall wave absorber" *M.S. Thesis*, Texas A&M University.
- Huygens, M., Verhoeven, R., Wachter, D.D., Himpe, J., Buyck, S., & Wens, F. (1994), "Underwater screens for shore protection" *Intl. Symp. Waves-Physical & Numerical Modeling*, Vancouver, Canada, 1503-1512.
- Isaacson, M. (1991), "Measurement of regular wave reflection" *ASCE J. of Waterway, Port, Coastal & Ocean Engineering*, Vol 117, 553-569.
- Isaacson, M., Whiteside, N., Gardiner, R., & Hay, D. (1994), "Modelling of a circular section floating breakwater" *Intl. Symp. Waves - Physical & Numerical Modeling*, Vancouver.

Kee, S. T. & Kim, M. H. (1997 March issue). "Flexible membrane wave barrier. Part 2. Floating/submerged buoy-membrane system." *ASCE J. of Waterway, Port, Coastal & Ocean Engineering*, (In Press).

Kim, M.H. & Kee, S.T. (1996) "Flexible membrane wave barrier. Part 1. Analytic and numerical solutions" *ASCE J. of Waterway, Port, Coastal & Ocean Engineering*, Vol.122, No.1, 46-53.

Lee, J.F. & Chen, C.J. (1990) "Wave interaction with hinged flexible breakwater" *J. of Hydraulic Research*, Vol 28, 283-295.

Ohyama, T., Tanaka, M., Kiyokawa, T., Uda, T., & Murai, Y. (1989) "Transmission and reflection characteristics of waves over a submerged flexible mound" *Coastal Engineering in Japan*, Vol.32, No.1, 53-68

Sawaragi, T., Aoki, S., & Yasui, A. (1989), "Tensions on silt curtains in currents and waves" *Proc. Offshore Mechanics & Arctic Engr. Conf.*, Hague, 13-21.

Seymour, R.J. & Hanes, D.M. (1979) "Performance analysis of tethered float breakwater" *ASCE J. of Waterway, Port, Coastal & Ocean Engineering*, Vol 105, #3, 265-281.

Sollitt, C.K., Lee, C.P., McDougal, W.G., & Perry, T.J. (1986) "Mechanically coupled buoyant flaps: theory and experiment" *Proc. 20th Coastal Engineering Conf.*, Vol.3, 2445-2459.

Thompson, G.O., Sollitt, C.K., McDougal, W.G. & Bender W.R. (1992) "Flexible membrane wave barrier" *ASCE Conf. Ocean V*, College Station, 129-148.

Wang, K.H. & Ren, X. (1993), "Water waves on a flexible and porous breakwater" *Journal of Engineering Mechanics*, Vol.119, 1025-1048.

Williams, A.N., Geiger, P.T., & McDougal, W.G. (1991), "Flexible floating breakwater" *ASCE J. of Waterway, Port, Coastal & Ocean Engineering*, Vol 117, #5, 429-450.

Williams, A.N., Geiger, P.T., & McDougal, W.G. (1992), "A submerged compliant breakwater" *J. of Offshore Mechanics & Arctic Engr.*, Vol 114, 83-90.

Zhao, R. (1994), "Hydroelastic analyses of a floating flexible body in waves" *9th Int. Workshop Water Waves & Floating Bodies*, Japan, 241-244.